Journal of Membrane Science 698 (2024) 122617

Contents lists available at ScienceDirect

Journal of Membrane Science

journal homepage: www.elsevier.com/locate/memsci

6FDA-polyimide thin-film composite hollow fiber membranes for hydrofluorocarbons and CO_2 separations

Sergio V. Gutiérrez-Hernández [a], Sandra Rico-Martínez [b], Fernando Pardo [a], Cristina Álvarez [c], Jesús A. Miguel [b], Gabriel Zarca [a,**], Ane Urtiaga [a,*]

[a] Dept. Chemical and Biomolecular Engineering, Universidad de Cantabria, Av. Los Castros 46, 39005, Santander, Spain
[b] Instituto Universitario CINQUIMA, University of Valladolid, Paseo Belén 5, 47011, Valladolid, Spain
[c] Instituto de Ciencia y Tecnología de Polímeros (ICTP - CSIC), Juan de La Cierva 3, 28006, Madrid, Spain

ARTICLE INFO

Keywords:
Fluorinated polyimides
Hollow fiber
Thin film composite membrane
Hydrofluorocarbons
R-32
CO_2

ABSTRACT

Herein, high molecular weight fluorinated aromatic polyimides were assessed for the first time to recover difluoromethane (R-32) from its blends with other hydrofluorocarbons and hydrofluoroolefins (R-134a: 1,1,1,2-tetrafluoroethane, R-125: pentafluoroethane, and R-1234yf: 2,3,3,3-tetrafluoropropene). First, a screening was performed with thick flat membranes made of the 4,4'-(hexafluoroisopropylidene)diphthalic anhydride (6FDA) and three different amines: 2,2'-bis(4-aminophenyl)hexafluoropropane (6FpDA), 2,4,6-trimethyl-m-phenylenediamine (TMPD), and 2,3,5,6-tetramethyl-1,3-phenyldiamine (durene). As a result, 6FDA-TMPD was selected for the fabrication of defect-free hollow fiber-thin film composite membranes (HF-TFCM) due to its superior performance for the separation of R-32. These HF-TFCMs showed excellent separation performance to reclaim high-purity R-32 (permeate concentration >99 vol%) from the commercial binary blends R-410A and R-454B (a mixture of R-32 and R-1234yf). In addition, we report for the first time the membrane recovery of R-32 from the ternary blend R-407C (R-32/R-134a/R-125 38.2:43.8:18 vol%). Eventually, the separation of CO_2 from synthetic gas mixtures of CO_2/CH_4 (50:50 vol%) and CO_2/N_2 (15:85 vol%) was performed for benchmarking, showing that the prepared HF-TFCM kept the separation performance of the 6FDA-TMPD thick membranes.

1. Introduction

Hydrofluorocarbons (HFCs) are a family of synthetic fluorinated gases (F-gases) mainly employed in the refrigeration and air-conditioning sectors (RAC). F-gases have become an issue of relevant concern due to their high global warming potential (GWP), e.g., the GWP of trifluoromethane (R-23) is 14,800 kg CO_2-eq per kg R-23, and their fugitive emissions to the atmosphere. The new regulations imposed on the production and consumption of F-gases [1,2] are shifting the RAC sector towards more sustainable approaches, such as the use of new low-GWP hydrofluoroolefins (HFOs), and the implementation of F-gas recycling aligned with a circular economy model [3]. In this context, boosting the reuse of the most valuable F-gases, recovered from RAC systems at their end of service, into new low GWP HFC/HFO refrigerants would avoid the incineration treatment and help to minimize the production of virgin F-gases.

However, refrigerant fluids typically exhibit near-azeotropic or azeotropic behavior, thus innovative separations are required to recover the individual compounds. In this regard, novel technologies based on absorption in ionic liquids (ILs) [4,5], adsorption in porous materials [6–9], and membranes [10–18] are being assessed for the separation of F-gas mixtures. In earlier works, we evaluated the permeability of F-gases in membranes prepared with poly(ether-block-amides (PEBA) and with polymers of intrinsic microporosity (PIM) [10,11,13–16]. Particularly, branched PIM-1 membranes showed excellent properties for separating difluoromethane (R-32) from R-410A and R-454B refrigerant blends, reaching R-32 permeability as high as 4100 barrer and exceptionally high selectivity, yet at the cost of losing functional properties over time due to the aging of the polymer membrane. Other glassy fluoropolymers such as PBVE-*co*-PDD [17,18], and PDD-VA [12] have been also evaluated for F-gas membrane separation.

In the search for the best polymer membrane materials for F-gas separations, we now explore the properties of fluorinated aromatic polyimides (PIs) based on 4,4'-(hexafluoroisopropylidene)diphthalic

* Corresponding author.
** Corresponding author.
E-mail addresses: zarcag@unican.es (G. Zarca), urtiaga@unican.es (A. Urtiaga).

https://doi.org/10.1016/j.memsci.2024.122617
Received 22 November 2023; Received in revised form 22 February 2024; Accepted 29 February 2024
Available online 1 March 2024

anhydride (6FDA). These aromatic fluorinated PIs can be easily synthesized by polycondensation between a diamine and the 6FDA dianhydride followed by a chemical or thermal cycloimidization process [19]. 6FDA-based PIs show good solubility in common organic solvents and can be easily processed into membranes with good mechanical properties [20,21]. Moreover, although the plasticization resistance and the mitigation of physical aging of fluorinated PIs still need to be improved to ensure a cost-effective membrane in long-term industrial operation [22,23], they exhibit lower physical aging than PIM-based membranes [24]. Furthermore, 6FDA-based PI membranes derived from 2,2′-bis(4-aminophenyl)hexafluoropropane (6FpDA), 2,4,6-trimethyl-*m*-phenylenediamine (TMPD) and 2,3,5,6-tetramethyl-1,3-phenyldiamine (durene) (Fig. 1) present an excellent balance between permeability and selectivity for the separation of conventional gas mixtures. For instance, these 6FDA-based PIs are known to present notable differences in CO_2 permeability; while the most flexible one, 6FDA-6FpDA, offers moderate CO_2 permeability (50–80 barrer) and good selectivity (19–25 for CO_2/N_2) [25–28], the most rigid ones, 6FDA-TMPD and 6FDA-durene, present higher CO_2 permeability (up to 1200 barrer) and lower selectivity (13–28 for CO_2/N_2) [29–35]. These three polyimides showed a similar trend in olefin/paraffin gas separation [28,36–38].

Overall, the good separation properties of fluorinated PIs towards CO_2 and the similar permeation behavior of difluoromethane (R-32) and CO_2 reported in previous works [13–16], led us to hypothesize that membranes fabricated with the 6FDA-based PIs could also display an exceptional performance for the separation of the valuable R-32 from HFCs and HFCs/HFOs refrigerant gas mixtures. The choice of 6FDA--based PIs was supported by the fact that the electronic and molecular volume characteristics of the hexafluoroisopropylidene group cause low chain packing, which results in high fractional free volume (FFV) polymers that may exhibit improved separation properties for separating mixtures of refrigerant gases [39]. Moreover, to date, membrane performance for F-gas separations has been evaluated only in flat membrane configuration, first at laboratory scale, and more recently, at pilot scale with Pebax®/ionic liquid thin-film composite membranes [11]. However, flat membranes present a low packing density of the membrane device, so their industrial application is operationally limited. To go further in the scale-up, the implementation of hollow fiber thin-film composite membranes (HF-TFCMs) is demanded to provide highly productive gas separation processes, with higher surface area and permeate production per unit [40]. Thus, in this work, HF-TFCMs were also prepared with the best-performing 6FDA-based polyimide, and the separation of the R-32 contained in the commercial blends R-410A, R–454B, and R-407C was assessed for first time in these HF-TFCMs. Moreover, this work also reports the CO_2 separation from its mixtures with methane and nitrogen, as a means for benchmarking the performance of these HF-TFCMs.

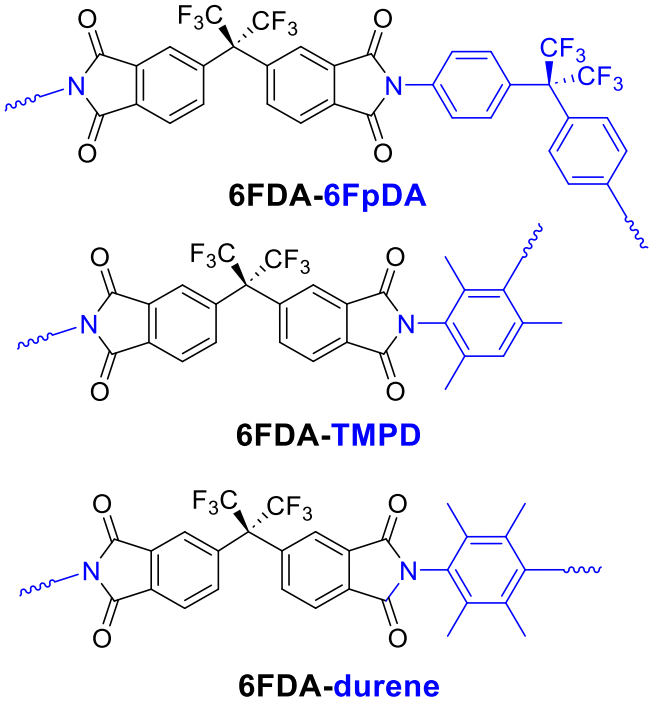

Fig. 1. Molecular configurations of the 6FDA-based polyimides employed in this work.

2. Materials and methods

A complete description of the polymer precursors, solvents, and gases used in this work is given in section S1.1 of the Supporting Information (SI). In addition, details of the methods employed for the characterization of the PI polymers (NMR, FTIR, TGA, DSC, WAXS, density, tensile tests, capillary flow porometry, and SEM/EDX) are reported in section S1.2 of the SI.

2.1. Synthesis of fluorinated polyimides

The three aromatic polyimides, 6FDA-6FpDA, 6FDA-TMPD, and 6FDA-durene were prepared by a two-step polycondensation reaction between 6FDA dianhydride and 6FpDA, TMPD, or durene diamine, by using the base-assisted in situ silylation method [28,41,42]. The detailed method and the complete characterization of the polyimides are described in the S1.3 and S2 sections of the SI, respectively.

2.2. Membrane preparation

The fluorinated PIs were casted as thick flat membranes from a 5% w/v solution of the polymer in tetrahydrofuran (THF) (500 mg in 10 mL of THF). The polymer solution was filtered using a 3.1 μm fiberglass filter, poured into a 9.2 cm glass ring located over a leveled glass plate, covered with a conical funnel, and left at room temperature overnight. The membranes were detached from the glass plate and subsequently exposed to thermal treatment: 100 °C (2 h), 125 °C (2 h), 150 °C (2 h), and 180 °C (12 h). The average thickness of the thick membranes was 38 μm (see Table S3). All PI membranes showed excellent mechanical properties, which are also collected in Table S3 of the SI.

2.3. Fabrication of 6FDA-based HF-TFCMs

The dip coating technique was applied for the preparation of 6FDA-TMPD HF-TFCM as described in Fig. 2, using polypropylene hollow fibers (3M™, Germany) as porous support (technical parameters collected in Table S4 and the pore size distribution in Fig. S12 of the SI). This approach minimizes the consumption of 6FDA-TMPD compared to the conventional dry-wet phase inversion process [43,44], hence making it more economically feasible for industrial implementation. Before the PI coating, one end of the PP support was potted with an epoxy resin (WEICON, Germany) to prevent polymer solution intrusion into the lumen of the hollow fiber. An automatic dip-coater, model ND-DC 300 (Nadetech Innovations, Spain) provided with a heating infrared system was used to optimize the reproducibility and scalability of the dip-coating process, allowing the accurate control of the soaking speed, soaking time, withdrawal speed, and drying time.

Firstly, the external surface of the PP porous support was impregnated with a highly permeable layer of PDMS (Sylgard® 184, 15 wt% in hexane) [45], which performed as a blocking layer to mitigate the intrusion of 6FDA-TMPD into the pores. Then, the PP HF was immersed in a 6FDA-TMPD solution. After each coating, the HF-TFCM was subjected to 0.5 min of infrared radiation for quick drying at 70 °C, followed

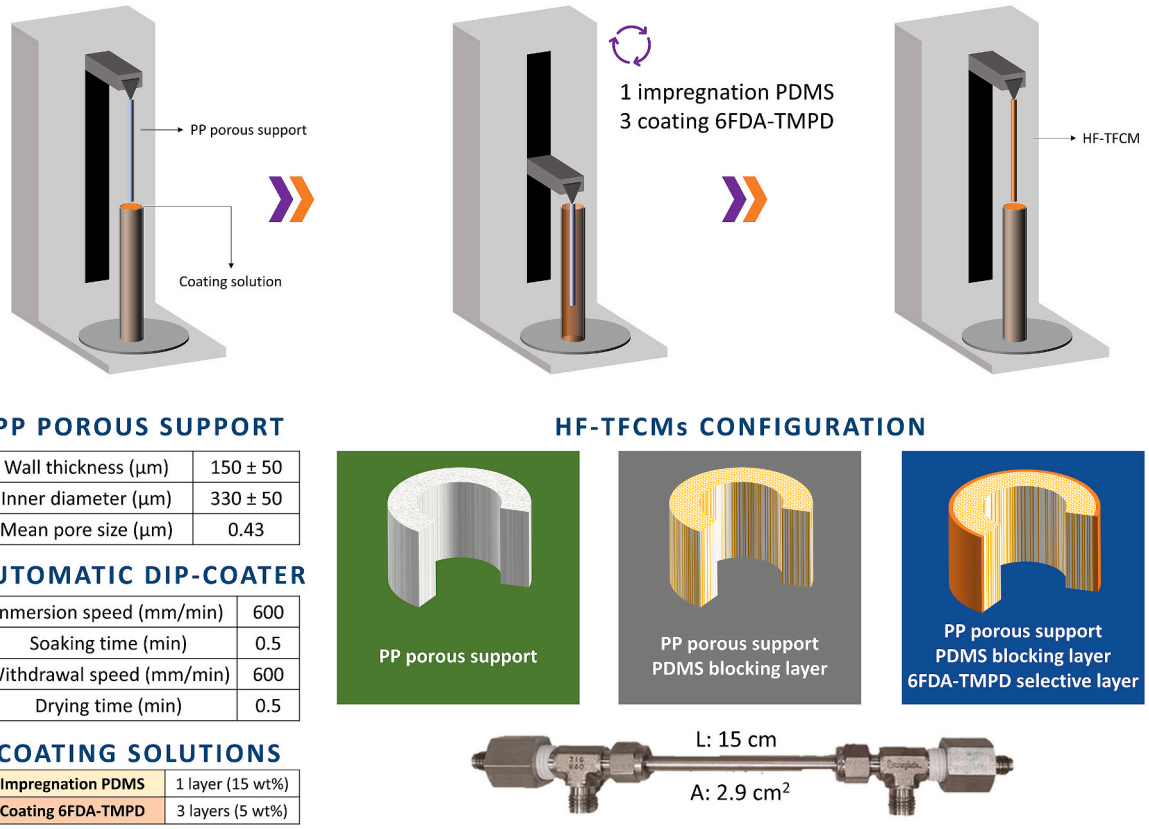

Fig. 2. Scheme of HF-TFCMs fabrication.

by 2 h drying at room temperature. Finally, one HF-TFCM (length of 15 cm) was assembled into a 1/4-inch stainless-steel tubular module, and potted with epoxy resin. The resulting membrane area in the HF device was 2.9 cm^2.

To ensure the reproducibility of the results reported with the prepared HF-TFCMs, the influence of several coating conditions on the separation properties of mixture R-410A was initially tested, namely, the concentration of the 6FDA-based polymer solution, the number of coating steps, the coating speeds, the drying time, and the PDMS concentration in solution were assessed. The optimized parameters of the dip coater for the deposition of the 6FDA-TMPD selective layer were: soaking speed, 600 mm min^{-1}; soaking time, 0.5 min; withdrawn speed, 600 mm min^{-1}; drying time: 0.5 min; whereas three coating cycles of 6FDA-TMPD solution at 5 wt % in THF were the best coating conditions to successfully achieve a defect-free selective coating of 6FDA-TMPD providing high gas permeance and excellent separation properties (see Fig. S13 of the SI).

2.4. Gas permeability and solubility measurements

The solution-diffusion model describes the gas permeability (P) through the dense 6FDA-based membranes, as the product of the solubility coefficient (S) and the diffusivity coefficient (D) (Equation (1)).

$$P = S \cdot D \tag{1}$$

The gas permeability measurements of 6FDA-based thick flat membranes were carried out in a custom-made permeation cell made of stainless steel employing 12.6 cm^2 circular membranes [10,11]. On the other hand, the gas permeability of HF-TFCMs was determined using the stainless-steel modules described in the previous section, feeding the gas into the lumen side of the HF membrane and collecting the permeate from the shell side. In both configurations (Fig. S1), the feed gas flow was maintained constant in a continuous flow of 20 cm^3_{STP} min^{-1} at 30 °C and the gas pressure (1.3–7.5 bar) was regulated using a backpressure transducer. The permeate was swept with an argon gas stream (2–10 cm^3_{STP} min^{-1}) and analyzed with a micro-gas chromatograph (Agilent 490) provided with two columns, molecular sieve and PoraPlot U, and a thermal conductivity detector (TCD). The permeate stream was continuously sampled over time by gas chromatography and the relative standard deviations concerning the reported average values were very low, always below 1%.

The gas permeability coefficient (P_i, barrer) was determined with Equation (2).

$$P_i = \frac{Q_i \cdot \delta}{A \cdot \left(f_{R,i} - f_{P,i}\right)} \tag{2}$$

where Q_i (cm^3_{STP} s^{-1}) is the permeate flow rate through the membrane, δ (cm) and A (cm^2) are the membrane thickness and effective permeation area, and $f_{P,i}$ (bar) and $f_{R,i}$ (bar) are the component fugacity in the permeate and retentate streams, respectively. For the HF-TFCMs, gas permeance (P_i/δ, 1 GPU $= 10^{-6}$ $\frac{cm^3_{STP}}{cm^2 \cdot s \cdot cmHg}$) was calculated instead of gas permeability. A detailed explanation of the fugacity calculation is given in section S1.4 of the SI.

The ideal gas permselectivity ($\alpha_{i/j}$) was calculated with Equation (3), and when the feed was a mixture, the separation factor ($SF_{i/j}$) was determined by means of Equation (4).

$$\alpha_{i/j} = \frac{P_i}{P_j} \tag{3}$$

$$SF_{i/j} = \frac{x_i^p \Big/ \sum_{j=1}^{n} x_j^p}{x_i^f \Big/ \sum_{j=1}^{n} x_j^f} \tag{4}$$

x_i and x_j denoted the molar fraction composition of the species i and $j(\neq i)$ in the binary or ternary mixtures, and the superscripts p and f designate the permeate and feed streams, respectively.

A custom-made sorption setup was used for determining the sorption isotherms of F-gases, CO_2, CH_4 and N_2 in 6FDA-TMPD flat membranes at 30 °C by the dual-volume pressure decay method as described in our previous works [10,13,15,16].

3. Results and discussion

3.1. 6FDA-based thick flat membranes

3.1.1. Screening of fluorinated PI for F-gas separation

A preliminary screening of the separation performance of the three PI membranes (6FDA-durene, 6FDA-TMPD, 6FDA-6FpDA) was performed under mixed-gas conditions at 30 °C and 3 bar, with the aim of selecting the best fluorinated PI for the fabrication of HF-TFCMs. In these experiments, the membrane cell was fed with the commercial blend R-410A (R-32/R-125, 69.7:30.3 vol%), a widespread near-azeotropic refrigerant blend that will be phased out in the near future due to its high content in R-125, a high-GWP HFC. The objective is to recover R-32, which is being implemented nowadays in RAC equipment as a substitute of R-410A.

Fig. 3 shows the permeability of each component (R-125 and R-32) and the separation factor of the mixture, while Table S5 of the SI collects all numerical data. Although all PI membranes presented relatively high FFV (6FDA-6FpDA: 0.133; 6FDA-TMPD: 0.151; 6FDA-durene: 0.169), the permeation results highlighted the important role of the diamine moieties on the separation properties of 6FDA-based PI membranes. The presence of methyl groups (-CH_3) in *ortho*-positions on the aromatic ring in the durene and TMPD diamine structures significantly increased the rotational rigidity of the macromolecular chain [46], leading to ineffective chain packing (increasing the FFV), which resulted in a high F-gas permeate flux due to enhanced gas diffusion and solubility coefficients [47]. Accordingly, 6FDA-durene exhibited the highest permeabilities, 62 and 5.6 barrer for R-32 and R-125, respectively, which agreed well with the rigid rotational restraint due to the presence of four methyl groups; whereas the trimethyl substitution of 6FDA-TMPD provided slightly lower permeabilities, 43 and 0.37 barrer for R-32 and R-125, respectively. However, 6FDA-durene yielded a lower separation

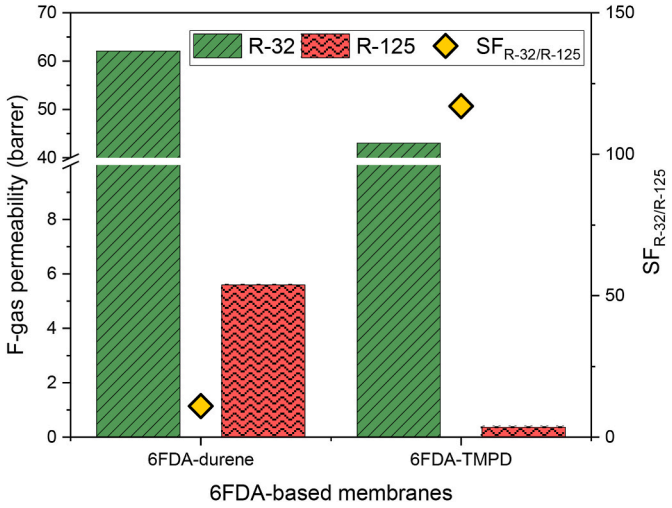

Fig. 3. Screening of mixed-gas permeability and separation factor of R-32 and R-125 through 6FDA-durene and 6FDA-TMPD thick flat membranes. The feed gas was R-410A (R-32/R-125 69.7:30.3 vol%) at 30 °C and 3 bar. The thick flat membranes were thermally treated as described in section 2.2. F-gas permeability through 6FDA-6FpDA was negligible in this experiment. Experimental data are collected in Table S5 of the SI.

factor ($SF_{R-32/R-125}$ = 11), compared to 6FDA-TMPD ($SF_{R-32/R-125}$ = 117), because its higher FFV produces a less selective material for the separation of the R-32/R-125 mixture [48]. In contrast, although the 6FpDA diamine contains bulky -CF_3 groups similar to those of 6FDA dianhydride, the 6FDA-6FpDA polyimide presents the lowest FFV, which led to a negligible F-gas permeability.

For all the above considerations, 6FDA-TMPD was selected as the best PI candidate for further evaluation of the F-gas separation properties and preparation of HF-TFCMs. In addition, these findings led us to determine that a good modulation of the free volume fraction of the membrane using techniques already developed in this field, could result in the formation of high-performance materials.

3.1.2. F-gas permeability through 6FDA-TMPD

In this section, the single gas permeation of F-gases was evaluated through 6FDA-TMPD thick flat membrane. On this occasion, the thick flat membrane was not subjected to the high-temperature treatment, to allow the comparison with the HF-TFCMs results that will be shown in the following section. It should be noted that the PP support used in the preparation of HF-TFCM does not allow heat treatments at the high temperatures required (180 °C) due to the lower melting temperature of PP (160–166 °C [49]).

First, the permeability of the pure gases CO_2, CH_4, N_2, and H_2 was determined at 30 °C and 1.3 bar (Table 1) for benchmarking the permeation properties of 6FDA-TMPD. The CO_2 gas permeability in 6FDA-TMPD membranes showed the highest value owing to the high sorption in 6FDA-TMPD (Fig. S14), and it was observed that the permeation rate decreased as the molecule kinetic diameter increased in the order H_2 (2.89 Å) > N_2 (3.64 Å) > CH_4 (3.8 Å). These permeability results were consistent with those previously reported in the literature (Table 1). However, it should be noted that the variation of both the casting solvent and the heat treatment during membrane formation had a clear effect on the transport properties of 6FDA-TMPD membranes [50]. The results compiled in Table 1 indicate that increasing the thermal treatment temperature induced densification of the membrane, resulting in an overall reduction of the gas permeability [51]. Nevertheless, the 6FDA-TMPD membranes without thermal treatment used in this section only showed moderately higher gas permeability coefficients (except for H_2) than those reported in previous works (see Table 1).

As the benchmarking results were consistent with those reported in the literature, the permeation properties of target F-gases (R-32, R-134a, R-1234yf, and R-125) were evaluated afterwards (Fig. 4). It is noteworthy that the R-32 permeability (P_{R-32} = 127 barrer) is up to three orders of magnitude higher than for the other F-gases studied, especially when compared to R-125 (P_{R-125} = 0.5 barrer). Also, the single gas permeability of R-32 was significantly higher than in the mixed gas results depicted in Fig. 3, a behavior that could be attributed mainly to the absence of heat treatment of the membrane. Again, these results revealed higher permeability values for the smallest F-gases, R-134a and R-32, and lower permeability for the biggest molecules, R-1234yf and R-125. This fact makes the 6FDA-TMPD membrane an ideal candidate for the selective separation of target F-gas systems, particularly for the most challenging separations R-32/R-1234yf (close-boiling mixture) and R-32/R-125 (close-boiling mixture with an azeotropic composition [56]), with ideal gas selectivity of 31.8 and 250, respectively. Thus, the separation performance of the 6FDA-TMPD membrane could promote the R-32 recovery from refrigerant blends and reuse it to formulate new low-GWP refrigerants [14]. Nevertheless, to gain in-depth understating of the permeability results, F-gas sorption experiments were done to clarify the main factor driving the permeation of these compounds through the 6FDA-TMPD membrane.

3.1.3. F-gas solubility in 6FDA-TMPD

As outlined above, the solution-diffusion mechanism controls the separation in 6FDA-TMPD membranes, so it is essential to assess the

Table 1
Gas permeation properties of 6FDA-TMPD thick flat membranes with different thermal treatments conditions and casting solvents.

Reference	Casting solvent	Thermal treatment (°C)	Operating conditions		Permeability (barrer)				Ideal gas selectivity	
			T (°C)	P (bar)	H_2	N_2	CO_2	CH_4	CO_2/N_2	CO_2/CH_4
This work	THF	–	30	1.3	344	31.8	645	29.1	20.6	22.6
[29]	NMP	100 (12 h)	25	6.9	n.a.	28.9	573	25.7	19.8	22.3
[52]	DCM	120 (24 h)	35	1	n.a.	n.a.	518	27.7	n.a.	18.7
[46]	DMF	200 (24 h)	35	2	407	25.3	498	23	19.7	21.7
[53]	DMAc	200 (20 h)	35	10	516	31.6	431	26	13.6	16.6
[54]	THF	270 (24 h)	35	2	n.a.	20.2	348	n.a.	17.2	n.a.
[55]	n.a.	387 (<1 h)	35	2	n.a.	17	299	15.1	17.6	19.8

THF: tetrahydrofuran; NMP: N-methyl-2-pyrrolidone; DCM: dichloromethane; DMF: N,N-dimethylformamide; DMAc: N,N-dimethylacetamide; n.a: not available.

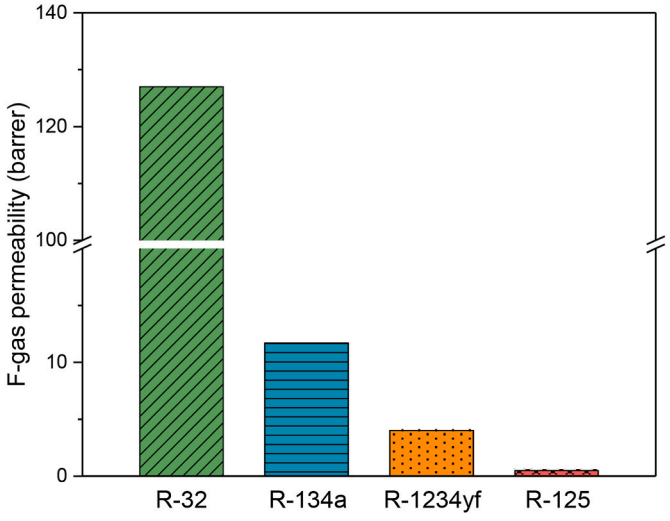

Fig. 4. Gas permeability of R-32, R-134a, R-1234yf, and R-125 through 6FDA-TMPD thick membrane at 30 °C and 1.3 bar. The membranes were not thermally treated after membrane casting. The permeability numerical values are collected in Table S6 of the SI.

contribution of each factor, solubility (S) and diffusivity (D), to the overall membrane permselectivity. To that end, gas solubility in 6FDA-TMPD thick flat membrane was evaluated obtaining the sorption isotherms of R-32, R-125, R-134a, and R-1234yf at 30 °C, which are shown in Fig. 5.

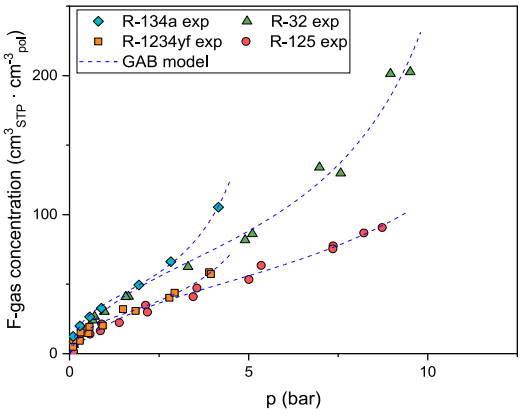

Fig. 5. Sorption isotherms of R-32, R-134a, R-1234yf, and R-125 in 6FDA-TMPD thick flat membrane at 30 °C. The dashed lines represent the GAB model results.

As can be seen, F-gas solubility in 6FDA-TMPD thick flat membrane followed IUPAC *type II* sorption isotherms [57], according to which the sorption takes place in a macroporous adsorbent with unrestricted monolayer-multilayer adsorption [58]. Firstly, at low pressures, the amount of adsorbed F-gas increased quickly because of the molecular interactions with 6FDA-TMPD. In accordance with the observed "sharp knee" region of the isotherms, multilayer formation began when the monolayer formation was completed, leading to the characteristic S-shaped isotherm indicating the bulk condensation of F-gas molecules inside the polymer matrix [59].

The results revealed that R-32 and R-134a were the most soluble F-gases in the 6FDA-TMPD matrix, whereas R-1234yf and R-125 were the least soluble. At the pressure of 1.3 bar, the F-gas concentration followed the order R-134a (40.4 $cm^3_{STP}\ cm^{-3}_{pol}$) > R-32 (37.2 $cm^3_{STP}\ cm^{-3}_{pol}$) > R-1234yf (26.7 $cm^3_{STP}\ cm^{-3}_{pol}$) > R-125 (24.0 $cm^3_{STP}\ cm^{-3}_{pol}$). Accordingly, the results showed excellent agreement with the trade-off between the condensability of the F-gas penetrant, which is linked to the solute critical temperature [60], and the kinetic diameter of the molecules (data collected in Table S1 of the SI). The combination of both parameters facilitated the gas adsorption within the polymeric membrane, being R-134a the most condensable (T_c = 374.18 K), and R-32 the smallest molecule (d_C = 4.02 Å), respectively. Furthermore, the adsorption tests were constrained by the vapor pressure of each F-gas, and it could be observed that the S-shape appeared when the pressure operation approached it. Accordingly, the sorption isotherms (Fig. 5) fitted perfectly ($R^2 > 0.99$) to the Guggenheim, Anderson, and de Boer (GAB) solubility model given by Equation (5).

$$C = \frac{v_m \cdot h \cdot p^* \cdot p}{(p^* - p)\cdot(h \cdot p + p^* - p)} \tag{5}$$

where C ($cm^3_{STP}\ cm^{-3}_{pol}$) is the equilibrium concentration of the solute, v_m ($cm^3_{STP}\ cm^{-3}_{pol}$) is the initial sorption layer capacity, h is the ratio of the adsorption strength in the initial and the consecutive layers, p^* (bar) is a pressure-independent constant and p is the equilibrium pressure (bar) [61]. The GAB model is generally applied for the description of CO_2 sorption in glassy polymers as an alternative to the dual mode sorption model (DMS) [62–64], and more recently, we applied it to describe the sorption of these highly condensable hydrofluorocarbons in membranes made of polymers of intrinsic microporosity [10]. The GAB model parameters were obtained for each F-gas by fitting the sorption experimental data to the model and reported in Table S7 of the SI.

From the permeability and solubility data at 1.3 bar and 30 °C, the contributions to the solubility and diffusivity permselectivity parameters were discerned. As can be seen in Table 2, the diffusivity selectivity (α_D) was the main factor controlling the separation in 6FDA-TMPD membranes, with the solubility selectivity (α_S) being close to 1 for the target pairs of F-gases evaluated. Overall, the single gas permeation and solubility results showed that 6FDA-TMPD stands out as a potential candidate to perform the challenging separation of azeotropic and near azeotropic F-gas mixtures such as R-32/R-125 and R-32/R-1234yf. Thus, in the next sections, 6FDA-TMPD HF-TFCMs were fabricated and their separation performance was assessed with the real blends R-410A,

Table 2
Permeability and solubility coefficients of single F-gases, and selectivity(α_P, α_S, α_D) for target F-gas mixtures in 6FDA-TMPD thick flat membranes, working at 30 °C and 1.3 bar.

F-gas	P (barrer)	S (cm^3_{STP} cm^{-3}_{pol} bar^{-1})	
R-32	125	28.6	
R-134a	11.9	31.6	
R-1234yf	4.03	20.5	
R-125	0.16	18.4	
F-gas pair	α_P	α_S	α_D
R-32/R-125	250	1.5	167
R-32/R-1234yf	31.2	1.4	22.3
R-32/R-134a	10.4	0.9	11.6

R-454B and R-407C.

Additional sorption experiments were performed with CO_2, N_2, and CH_4 at 30 °C (Fig. S14 of the SI). The CO_2 concentration at 1.3 bar was 19.6 (cm^3_{STP} cm^{-3}_{pol}), which is half that of R-32 (37.2 cm^3_{STP} cm^{-3}_{pol}) at the same pressure. In contrast, CO_2 permeability was 5-fold higher than R-32 ($P_{CO2} = 645$ and $P_{R-32} = 127$ barrer), owing to the smaller molecular size of CO_2, clearly remarking the role of diffusivity in the gas separation mechanism.

3.2. Preparation and characterization of 6FDA-TMPD hollow fiber thin film composite membranes (HF-TFCMs)

HF-TFCM fabrication was followed by FTIR-ATR analysis between each step to ensure proper deposition of each coating layer over the PP support (Fig. 6a). First, the PP support was characterized as the base material of HF-TFCMs. The absorption bands displayed at 2836-2948 cm^{-1} were attributed to the stretching vibrations of the C–H bond (2948 cm^{-1} asymmetric -CH_3, 2920 cm^{-1} asymmetric -CH_2-, 2868 cm^{-1} symmetric -CH_3, 2836 cm^{-1} symmetric -CH_2-) [65]. Moreover, the bending vibrations of the methylene (–CH_2–) and methyl (-CH_3) groups were observed at 1456 cm^{-1} and 1376 cm^{-1}, respectively [66]. After the PDMS impregnation, the characteristic peaks of this polymer appeared in the spectrum, e.g., the stretching vibration of Si–C in -Si–CH_3 group at 800 cm^{-1} and Si–O–Si at 1076 cm^{-1}. Also, the band appearing at 1260 cm^{-1} was due to the symmetric -CH_3 in Si–CH_3 [67,68]. Finally, after the deposition of 6FDA-TMPD, the spectrum confirmed that the selective polyimide layer was satisfactorily deposited onto the porous support. This spectrum corresponded to that of the flat 6FDA-TMPD membrane, also shown in Fig. 6a, with the characteristic peaks of the imide group at

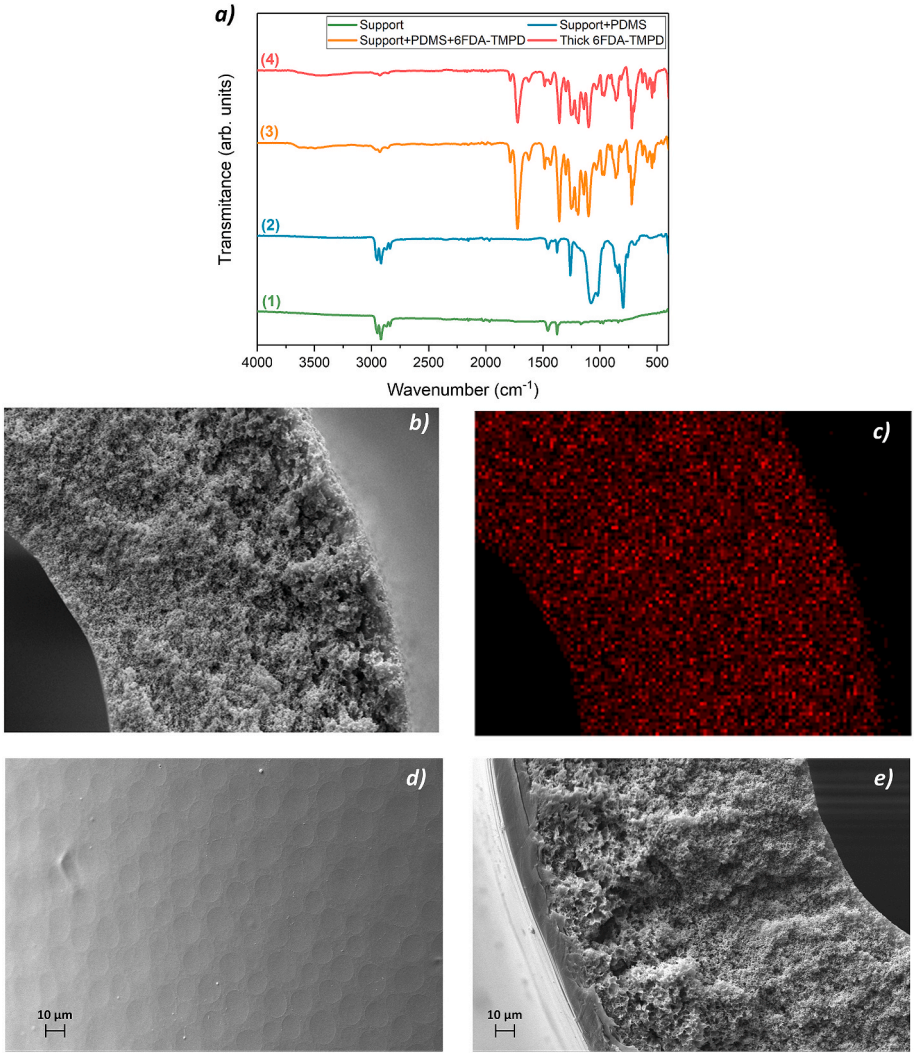

Fig. 6. A) FTIR spectra of (1) PP HF support, (2) PP HF support + PDMS impregnation, (3) PP HF support + PDMS impregnation + 3 coatings of 6FDA-TMPD, and (4) 6FDA-TMPD thick flat membrane; b) cross-section SEM images of PP/PDMS HF; c) cross-section silicon mapping (EDX) PP/PDMS HF; d) external surface 6FDA-TMPD HF-TFCM; e) cross-section SEM image of 6FDA-TPMD HF-TFCM. (For interpretation of the references to colour in this figure legend, the reader is referred to the Web version of this article.)

1784 cm^{-1} (asymmetric C═O stretching), 1720 cm^{-1} (symmetric C═O stretching), 1356 cm^{-1} (C–N stretching) [28,69] and the imide ring deformation at 720 cm^{-1} [70].

In addition, the HF-TFCM fabrication was characterized by SEM and EDX images. Fig. 6b shows the cross section of the PP fiber impregnated with PDMS, where it can be observed that PDMS was not deposited on the external PP surface forming a dense layer. In contrast, EDX characterization (Fig. 6c) showed a distribution of silicon through the fiber cross section, indicating that the PDMS was embedded within the PP matrix forming a blocking layer that prevented the intrusion of 6FDA-TMPD into the membrane pores. The HFs impregnated with PDMS showed high gas permeance (N_2: 7022 GPU, CO_2: 7227 GPU) and non-selective properties ($\propto_{CO_2/N_2} \approx 1$). To assess the influence of PDMS on these results, the air flow through the PP fiber was also determined in a porometer (Porometer 3G, Anton Paar) leading to a much higher permeance of $1.85 \cdot 10^5$ GPU due to its macroporous nature. Thus, the separation properties of the HF-TFCMs discussed in the following sections will be attributed exclusively to the top layer of 6FDA-TMPD. Nevertheless, we checked that the PDMS impregnation was required in order to coat a defect-free layer of 6FDA-TMPD on top of the PP support. Finally, Fig. 6d shows the external surface layer of 6FDA-TMPD, highlighting its dense morphology, and Fig. 6e shows the cross section in which a thickness of the 6FDA-TMPD selective thin film layer can be identified (between 6 and 7 μm).

3.3. 6FDA-TMPD HF-TFCMs mixed-gas separation performance

3.3.1. Separation of commercial refrigerant blends

Considering the high permeability and selectivity of the 6FDA-TMPD flat membrane towards single F-gases, mixed F-gas experiments were addressed for the first time with the HF-TFCMs at 1.3 bar and 30 °C. The results are shown in Fig. 7 for the commercial refrigerant mixtures R-410A, R-454B, and R-407C, all three including R-32 in their composition.

Regarding the separation of the R-410A mixture, R-32 permeance was 13.9 GPU with a R-32/R-125 separation factor of 78.5, 2-fold higher than in our earlier research work dealing with PIM-1 membranes [10] and 3-fold higher than the results reported with the 50% PBVE- 50% PDD copolymer [17]. As a result, the R-32 concentration in the permeate stream, excluding the argon sweep gas, reached the exceptional concentration of 99.45 vol%, the highest permeate purity of R-32 ever obtained for the feed R-410A (R-32 and R-125 50 % wt. each gas) by applying advanced membrane separation processes. Likewise, for the mixture R-454B, the R-32 permeance was slightly higher (14.7 GPU) and the $SF_{R-32/\ R-1234yf} = 34$, together with a final R-32 concentration in the permeate stream of 99.40 vol%. These results outperformed our previous work with thin-film composite polymer/ionic liquid membranes in pilot scale experiments [11], where 89.63 and 95.93 vol% R-32 permeate streams were obtained from R-410A and R-454B, respectively. Fig. 7 also includes the performance of the highly selective 6FDA-TMPD HF-TFCM in the separation of R-407C, a ternary refrigerant composed of R-32, R-134a, and R-125 (38.2:43.8:18.0 vol%). The R-32 permeance was 10.9 GPU with a $SF_{R-32/(R-134a+R-125)} = 14.4$. This result is very promising because it shows the great potential of 6FDA-TMPD membranes to recover R-32 (90 vol% R-32 in the permeate, in a single permeation stage) even from a ternary mixture with an initial concentration of only 38.2 vol% R-32.

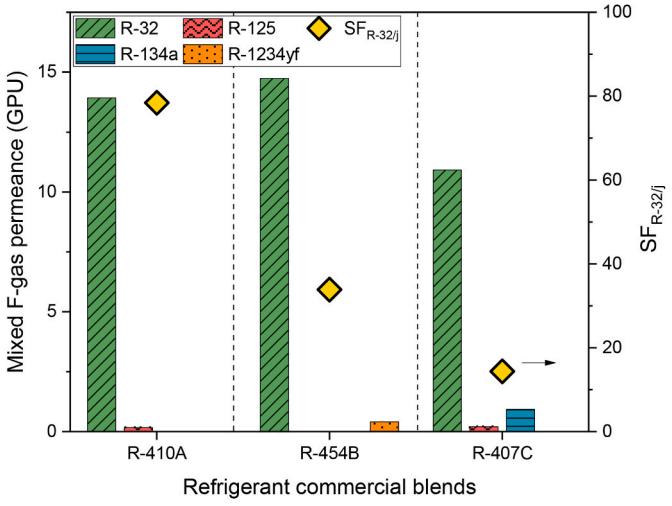

Fig. 7. Mixed-gas separation performance of 6FDA-TMPD HF-TFCM at 30 °C and 1.3 bar. Permeance (left-hand y-axis) vs. separation factor (right-hand y-axis) towards R-32 with respect to other F-gases (R-410A: j = R-125; R-454B: j = R-1234yf; R-407C: j = R-134a + R-125). The feed stream compositions were R-410A (R-32/R-125 69.7:30.3 vol%), R-454B (R-32/R-1234yf 82.9:17.1 vol %), R-407C (R-32/R-134a/R-125 38.2:43.8:18 vol%).

3.3.2. Pressure effect

To fully understand the behavior of 6FDA-TMPD HF-TFCMs under real process conditions, the pressure dependence of R-32 and R-125 was evaluated under mixed-gas conditions (mixture R-410A) in the range 1.3–7.5 bar at 30 °C. The R-32 and R-125 permeances, results plotted in Fig. 8, decreased with increasing feed pressure up to 2.5 bar, and subsequently showed an upward rate at higher feed pressures. These results are indicative of a plasticization phenomenon [71], which has already been reported during CO_2 permeation in 6FDA-TMPD membranes [31], as well as in our previous work with PIM-1 membranes [10]. As noted earlier, the high solubility of the condensable R-32 promoted the polymer chain mobility resulting in an increase of diffusion through the membrane, which turned into the permeance increase of R-32 and R-125 with increasing pressure. Therefore, the major drawback of plasticization was the decline of the separation performance due to the loss of the size discrimination ability of the PI membrane [72]. However, despite the plasticization phenomenon, it was seen that when the feed pressure was further increased up to 7.5 bar, the R-32 permeance (30 GPU) was 4-fold higher than the initial permeance at 1.3 bar, reaching a separation factor $\propto_{R-32/R-125}$ of 7, and a permeate concentration of 94.30 vol% of R-32.

3.3.3. CO_2 separations

The separation performance of 6FDA-TMPD HF-TFCMs was also

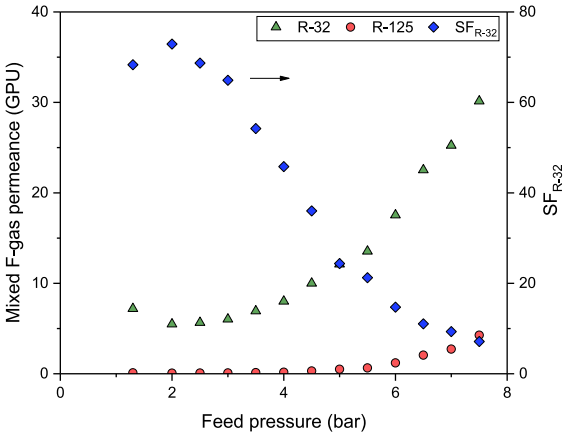

Fig. 8. Pressure dependence R-32 and R-125 mixed-gas permeability using R-410A (70 vol% R-32/30 vol% R-125) as feed gas at 30 °C through 6FDA-TMPD-based HF-TFCM. Experimental data are collected in Table S9 of the SI.

evaluated with synthetic mixtures emulating the composition of relevant applications, such as biogas upgrading (CO_2/CH_4 50:50 vol%) and flue gas separation (CO_2/N_2 15:85 vol%) for benchmarking (Fig. 9). Moderately good CO_2 permeance (99.7 GPU) was attained working with CO_2/N_2 mixture (15:85 vol%), reaching a CO_2 concentration in the permeate of 81.5 vol%, a considerable enrichment from the initial 15 vol % CO_2 in the feed ($SF_{CO2/N2} = 24.8$). On the other hand, for the separation of CO_2/CH_4 mixture (50:50 vol%), lower CO_2 permeance was achieved, 54.5 GPU, leading to a CO_2 permeate concentration of 93.3 vol % ($SF_{CO2/CH4} = 13.9$). Despite having a thicker selective layer, the CO_2 permeance of the 6FDA-TMPD HF-TFCM in this work was very similar to that reported by Liu et al. [73], who developed the first 6FDA-TMPD: DABA (3:2) asymmetric hollow fibers by dry-jet/wet-quench approach. The HF-TFCM prepared in the present study exhibited the expected CO_2 separation performance of 6FDA-TMPD reported with pure gases (Table 1), thus indicating that the separation properties of this PI have been successfully transferred from the thick flat membranes to the HF-TFCMs. This shows that optimizing the coating procedure to obtain thinner selective layers could lead to high-productivity gas separation membranes while minimizing the required amount of the 6FDA--based PIs.

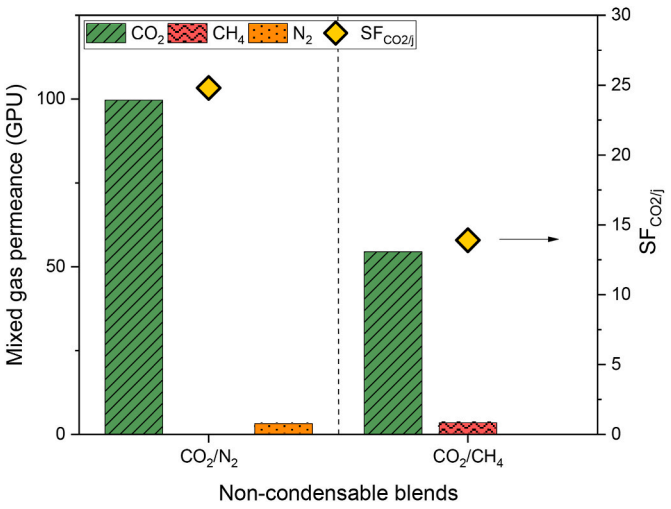

Fig. 9. Mixed-gas separation performance of 6FDA-TMPD HF-TFCM at 30 °C and 1.3 bar. Permeance of non-condensable gases (left-hand y-axis) vs. CO_2/N_2 or CO_2/CH_4 separation factor (right-hand y-axis). The feed stream compositions were CO_2/CH_4 (50:50 vol%) and CO_2/N_2 (15:85 vol%). Experimental data are collected in Table S10 of the SI.

4. Conclusions

This work has explored the unprecedented separation performance of 6FDA-based fluorinated polyimides for the separation of close-boiling refrigerant blends by tuning the diamine structures of the aromatic polyimides. Among them, 6FDA-TMPD showed excellent permeability-selectivity trade-off for the separation of difluoromethane (R-32) from other hydrofluorocarbons, which was mostly attributed to a diffusion-controlled mechanism. Thus, thin-film composite hollow fiber membranes (HF-TFCMs) with a defect-free dense layer of 6FDA-TMPD were successfully prepared using a dip coating methodology over a polypropylene support. These membranes allowed the successful recovery of the valuable R-32 (>99.4 vol% permeate concentration) from binary mixtures of close-boiling hydrofluorocarbons and hydrofluoroolefins. These results outperformed the values of other membrane materials described in the literature. Similarly, moderate CO_2 mixed-gas permeances were achieved in CO_2/N_2 and CO_2/CH_4 separations, which are equivalent to those previously reported through other 6FDA-based asymmetric hollow fiber membranes prepared by phase inversion. Therefore, these results showed the great potential of 6FDA-TMPD for developing HF membranes via dip coating by using a low amount of costly high-performance specialty polymers such as the fluorinated polyimides employed in this work. Future research efforts should focus on optimizing the coating procedure to minimize the dense selective layer thickness to obtain high-productivity 6FDA-TMPD HF-TFCMs materials.

CRediT authorship contribution statement

Sergio V. Gutiérrez-Hernández: Writing – original draft, Investigation, Formal analysis. **Sandra Rico-Martínez:** Writing – original draft, Investigation, Formal analysis. **Fernando Pardo:** Investigation, Formal analysis. **Cristina Álvarez:** Writing – review & editing, Investigation, Formal analysis. **Jesús A. Miguel:** Writing – review & editing, Supervision, Funding acquisition. **Gabriel Zarca:** Writing – review & editing, Supervision, Conceptualization. **Ane Urtiaga:** Writing – review & editing, Supervision, Project administration, Funding acquisition, Conceptualization.

Declaration of competing interest

The authors declare that they have no known competing financial interests or personal relationships that could have appeared to influence the work reported in this paper.

Data availability

All data are included in the supporting Information file

Acknowledgments

We kindly acknowledge the funding of projects PID2019-105827RB-I00, PID2022-138028OB-I00, PID2020-118547GB-I100, PID2019-109403RB-C22, PID2019-109403RB-C21 by the Spanish State Research Agency and partially by the European Fund for Regional Development (EU), and the Regional Government of Castilla y León (project VA224P20). F.P., S.V.G.H. and S.R.M acknowledge the support of the Spanish State Research Agency and the Spanish Ministry of Science and Innovation (grants IJC2020-043134-I, PRE2020-093568 and, FPU2019/05446 respectively). All authors kindly thank Dr. Ángel E. Lozano for his advice with the selection of polymers and his helpful discussions and support. We would also like to thank 3M Company for generous donation of polypropylene hollow fibers.

Appendix A. Supplementary data

Supplementary data to this article can be found online at https://doi.org/10.1016/j.memsci.2024.122617.

References

[1] E.A. Heath, Amendment to the Montreal Protocol on substances that deplete the ozone layer (Kigali Amendment), Int. Leg. Mater. 56 (2017) 193–205, https://doi.org/10.1017/ILM.2016.2.
[2] Regulation (EU), No 517/2014 of the European Parliament and of the Council of 16 April 2014 on fluorinated greenhouse gases and repealing Regulation (EC), European Environment Agency 842 (2006). https://www.eea.europa.eu/policy-documents/regulation-eu-no-517-2014. (Accessed 12 September 2023).
[3] P.J. Castro, J.M.M. Aráujo, G. Martinho, A.B. Pereiro, Waste management strategies to mitigate the effects of fluorinated greenhouse gases on climate change, Appl. Sci. 11 (2021) 4367, https://doi.org/10.3390/APP11104367. Page 4367 11 (2021).
[4] S. Asensio-Delgado, M. Viar, F. Pardo, G. Zarca, A. Urtiaga, Gas solubility and diffusivity of hydrofluorocarbons and hydrofluoroolefins in cyanide-based ionic liquids for the separation of refrigerant mixtures, Fluid Phase Equil. 549 (2021) 113210, https://doi.org/10.1016/J.FLUID.2021.113210.
[5] M. Viar, S. Asensio-Delgado, F. Pardo, G. Zarca, A. Urtiaga, In the quest for ionic liquid entrainers for the recovery of R-32 and R-125 by extractive distillation under

rate-based considerations, Sep. Purif. Technol. 324 (2023) 124610, https://doi.org/10.1016/J.SEPPUR.2023.124610.
[6] J.E. Sosa, C. Malheiro, R.P.P.L. Ribeiro, P.J. Castro, M.M. Piñeiro, J.M.M. Araújo, F. Plantier, J.P.B. Mota, A.B. Pereiro, Adsorption of fluorinated greenhouse gases on activated carbons: evaluation of their potential for gas separation, J. Chem. Technol. Biotechnol. 95 (2020) 1892–1905, https://doi.org/10.1002/JCTB.6371.
[7] J.E. Sosa, P.J. Castro, R.P.P.L. Ribeiro, J.P.B. Mota, J.M.M. Araújo, A.B. Pereiro, C. Malheiro, F. Plantier, M.M. Piñeiro, Exploring the potential of metal–organic frameworks for the separation of blends of fluorinated gases with high global warming potential, Global Challenges 7 (2023) 2200107, https://doi.org/10.1002/GCH2.202200107.
[8] A.D. Yancey, D.P. Broom, M.G. Roper, M.J. Benham, D.R. Corbin, M.B. Shiflett, Separation of azeotropic hydrofluorocarbon refrigerant mixtures: thermodynamic and kinetic modeling for binary adsorption of HFC-32 and HFC-125 on zeolite 5A, Langmuir 38 (2022) 10836–10853, https://doi.org/10.1021/ACS.LANGMUIR.2C01491.
[9] A.D. Yancey, D.R. Corbin, M.B. Shiflett, Difluoromethane (HFC-32) and pentafluoroethane (HFC-125) sorption on linde type A (LTA) zeolites for the separation of azeotropic hydrofluorocarbon refrigerant mixtures, Langmuir 38 (2022) 1937–1953, https://doi.org/10.1021/ACS.LANGMUIR.1C02904.
[10] S.V. Gutiérrez-Hernández, F. Pardo, A.B. Foster, P. Gorgojo, P.M. Budd, G. Zarca, A. Urtiaga, Outstanding performance of PIM-1 membranes towards the separation of fluorinated refrigerant gases, J. Membr. Sci. 675 (2023) 121532, https://doi.org/10.1016/J.MEMSCI.2023.121532.
[11] F. Pardo, S.V. Gutiérrez-Hernández, P. Rodríguez-San Miguel, G. Zarca, A. Urtiaga, Polymer/ionic liquid pilot scale membrane prototype for the recovery of difluoromethane (R-32) from refrigerant mixtures, Sep. Purif. Technol. 320 (2023) 124115, https://doi.org/10.1016/J.SEPPUR.2023.124115.
[12] A.N. Harders, S. Dixon, B. Hines, M. Lundin, W. White, M.B. Shiflett, Separation of refrigerant gases using a copolymer of perfluoro(2,2-dimethyl-1,3-dioxole) (PDD) and vinyl acetate (VA), Ind. Eng. Chem. Res. (2023), https://doi.org/10.1021/ACS.IECR.3C01822.
[13] F. Pardo, G. Zarca, A. Urtiaga, Separation of refrigerant gas mixtures containing R32, R134a, and R1234yf through poly(ether- block-amide) membranes, ACS Sustain. Chem. Eng. 8 (2020) 2548–2556, https://doi.org/10.1021/ACSSUSCHEMENG.9B07195.
[14] F. Pardo, G. Zarca, A. Urtiaga, Effect of feed pressure and long-term separation performance of Pebax-ionic liquid membranes for the recovery of difluoromethane (R32) from refrigerant mixture R410A, J. Membr. Sci. 618 (2021) 118744, https://doi.org/10.1016/J.MEMSCI.2020.118744.
[15] F. Pardo, S.V. Gutiérrez-Hernández, G. Zarca, A. Urtiaga, Toward the recycling of low-GWP hydrofluorocarbon/hydrofluoroolefin refrigerant mixtures using composite ionic liquid-polymer membranes, ACS Sustain. Chem. Eng. 9 (2021) 7012–7021, https://doi.org/10.1021/ACSSUSCHEMENG.1C00668.
[16] F. Pardo, S.V. Gutiérrez-Hernández, C. Hermida-Merino, J.M.M. Araújo, M. M. Piñeiro, A.B. Pereiro, G. Zarca, A. Urtiaga, Integration of stable ionic liquid-based nanofluids into polymer membranes. Part II: gas separation properties toward fluorinated greenhouse gases, Nanomaterials 11 (2021) 582, https://doi.org/10.3390/NANO11030582. Page 582 11 (2021).
[17] A.N. Harders, E.R. Sturd, L. Wallisch, H. Schmidt, Y. Mendoza-Apodaca, D. R. Corbin, W. White, C.P. Junk, M.B. Shiflett, Solubility, diffusivity, and permeability of HFC-32 and HFC-125 in amorphous copolymers of perfluoro (butenyl vinyl ether) and perfluoro(2,2-dimethyl-1,3-dioxole), Ind. Eng. Chem. Res. 62 (2023) 4054–4063, https://doi.org/10.1021/ACS.IECR.2C04518.
[18] A.N. Harders, E.R. Sturd, J.E. Vallier, D.R. Corbin, W.R. White, C.P. Junk, M. B. Shiflett, Selective separation of HFC-32 from R-410A using poly (dimethylsiloxane) and a copolymer of perfluoro(butenyl vinyl ether) and perfluoro(2,2-dimethyl-1,3-dioxole), J. Membr. Sci. 652 (2022) 120467, https://doi.org/10.1016/J.MEMSCI.2022.120467.
[19] H. Sanaeepur, A. Ebadi Amooghin, S. Bandehali, A. Moghadassi, T. Matsuura, B. Van der Bruggen, Polyimides in membrane gas separation: monomer's molecular design and structural engineering, Prog. Polym. Sci. 91 (2019) 80–125, https://doi.org/10.1016/J.PROGPOLYMSCI.2019.02.001.
[20] M.Z. Ahmad, P. Izak, V. Fila, CO2 separation of fluorinated 6FDA-based polyimides, performance-improved ZIF-incorporated mixed matrix membranes and gas permeability model evaluations, J. Environ. Chem. Eng. 10 (2022) 108611, https://doi.org/10.1016/J.JECE.2022.108611.
[21] V.I. Bonder, B.D. Freeman, Y.P. Yampolskii, Sorption of gases and vapors in an amorphous glassy perfluorodioxole copolymer, Macromolecules 32 (1999) 6163–6171, https://doi.org/10.1021/MA9817222.
[22] J.D. Wind, S.M. Sirard, D.R. Paul, P.F. Green, K.P. Johnston, W.J. Koros, Carbon dioxide-induced plasticization of polyimide membranes: pseudo-equilibrium relationships of diffusion, sorption, and swelling, Macromolecules 36 (2003) 6433–6441, https://doi.org/10.1021/MA0343582.
[23] M. Houben, M. van Essen, K. Nijmeijer, Z. Borneman, Time-dependent plasticization behavior of polyimide membranes at supercritical conditions, J. Membr. Sci. 635 (2021) 119512, https://doi.org/10.1016/J.MEMSCI.2021.119512.
[24] T.H. Lee, M. Balçık, B.K. Lee, B.S. Ghanem, I. Pinnau, H.B. Park, Hyperaging-induced H2-selective thin-film composite membranes with enhanced submicroporosity toward green hydrogen supply, J. Membr. Sci. 672 (2023) 121438, https://doi.org/10.1016/J.MEMSCI.2023.121438.
[25] W.J. Koros, D.R.B. Walker, Gas separation membrane material selection criteria: weakly and strongly interacting feed component situations, Polym. J. 23 (1991) 481–490, https://doi.org/10.1295/polymj.23.481.
[26] K. Tanaka, H. Kita, M. Okano, K. ichi Okamoto, Permeability and permselectivity of gases in fluorinated and non-fluorinated polyimides, Polymer 33 (1992) 585–592, https://doi.org/10.1016/0032-3861(92)90736-G.
[27] R. Recio, L. Palacio, P. Prádanos, A. Hernández, Á.E. Lozano, Á. Marcos, J.G. de la Campa, J. de Abajo, Gas separation of 6FDA–6FpDA membranes: effect of the solvent on polymer surfaces and permselectivity, J. Membr. Sci. 293 (2007) 22–28, https://doi.org/10.1016/J.MEMSCI.2007.01.022.
[28] S. Rico-Martínez, C. Álvarez, A. Hernández, J.A. Miguel, Á.E. Lozano, Mixed matrix membranes loaded with a porous organic polymer having bipyridine moieties, Membranes 12 (2022) 547, https://doi.org/10.3390/MEMBRANES12060547/S1.
[29] S. Xu, X. Ren, N. Zhao, L. Wu, Z. Zhang, Y. Fan, N. Li, Self-crosslinking of bromomethylated 6FDA-DAM polyimide for gas separations, J. Membr. Sci. 636 (2021) 119534, https://doi.org/10.1016/J.MEMSCI.2021.119534.
[30] S. Xu, N. Zhao, L. Wu, S. Kang, Z. Zhang, G. Huo, Z. Dai, N. Li, Carbon molecular sieve gas separation membranes from crosslinkable bromomethylated 6FDA-DAM polyimide, J. Membr. Sci. 659 (2022) 120781, https://doi.org/10.1016/J.MEMSCI.2022.120781.
[31] W. Qiu, L. Xu, C.C. Chen, D.R. Paul, W.J. Koros, Gas separation performance of 6FDA-based polyimides with different chemical structures, Polymer 54 (2013) 6226–6235, https://doi.org/10.1016/J.POLYMER.2013.09.007.
[32] C. Álvarez, A.E. Lozano, J.G. de la Campa, High-productivity gas separation membranes derived from pyromellitic dianhydride and nonlinear diamines, J. Membr. Sci. 501 (2016) 191–198, https://doi.org/10.1016/J.MEMSCI.2015.11.039.
[33] S. Sato, T. Ose, S. Miyata, S. Kanehashi, H. Ito, S. Matsumoto, Y. Iwai, H. Matsumoto, K. Nagai, Relationship between the gas transport properties and the refractive index in high-free-volume fluorine-containing polyimide membranes, J. Appl. Polym. Sci. 121 (2011) 2794–2803, https://doi.org/10.1002/APP.33784.
[34] S. Miyata, S. Sato, K. Nagai, T. Nakagawa, K. Kudo, Relationship between gas transport properties and fractional free volume determined from dielectric constant in polyimide films containing the hexafluoroisopropylidene group, J. Appl. Polym. Sci. 107 (2008) 3933–3944, https://doi.org/10.1002/APP.27496.
[35] D. Wu, B. Zhang, J. Yuan, C. Yi, Structural engineering on 6FDA-Durene based polyimide membranes for highly selective gas separation, Sep. Purif. Technol. 316 (2023) 123786, https://doi.org/10.1016/J.SEPPUR.2023.123786.
[36] C. Staudt-Bickel, W.J. Koros, Olefin/paraffin gas separations with 6FDA-based polyimide membranes, J. Membr. Sci. 170 (2000) 205–214, https://doi.org/10.1016/S0376-7388(99)00351-8.
[37] M. Das, W.J. Koros, Performance of 6FDA–6FpDA polyimide for propylene/propane separations, J. Membr. Sci. 365 (2010) 399–408, https://doi.org/10.1016/J.MEMSCI.2010.09.029.
[38] C. Zhang, Y. Dai, J.R. Johnson, O. Karvan, W.J. Koros, High performance ZIF-8/6FDA-DAM mixed matrix membrane for propylene/propane separations, J. Membr. Sci. 389 (2012) 34–42, https://doi.org/10.1016/J.MEMSCI.2011.10.003.
[39] Y. Yampolskii, N. Belov, A. Alentiev, Perfluorinated polymers as materials of membranes for gas and vapor separation, J. Membr. Sci. 598 (2020) 117779, https://doi.org/10.1016/J.MEMSCI.2019.117779.
[40] G. Li, W. Kujawski, R. Válek, S. Koter, A review - the development of hollow fibre membranes for gas separation processes, Int. J. Greenh. Gas Control 104 (2021) 103195, https://doi.org/10.1016/J.IJGGC.2020.103195.
[41] D.M. Muñoz, M. Calle, J.G. De La Campa, J. De Abaje, A.E. Lozane, An improved method for preparing very high molecular weight polyimides, Macromolecules 42 (2009) 5892–5894, https://doi.org/10.1021/MA9005268.
[42] D.M. Muñoz, J.G. De La Campa, J. De Abajo, A.E. Lozano, Experimental and theoretical study of an improved activated polycondensation method for aromatic polyimides, Macromolecules 40 (2007) 8225–8232, https://doi.org/10.1021/MA070842J.
[43] C. Zhang, K. Zhang, L. Xu, Y. Labreche, B. Kraftschik, W.J. Koros, Highly scalable ZIF-based mixed-matrix hollow fiber membranes for advanced hydrocarbon separations, AIChE J. 60 (2014) 2625–2635, https://doi.org/10.1002/AIC.14496.
[44] L. Xu, C. Zhang, M. Rungta, W. Qiu, J. Liu, W.J. Koros, Formation of defect-free 6FDA-DAM asymmetric hollow fiber membranes for gas separations, J. Membr. Sci. 459 (2014) 223–232, https://doi.org/10.1016/J.MEMSCI.2014.02.023.
[45] C.Z. Liang, T.S. Chung, Robust thin film composite PDMS/PAN hollow fiber membranes for water vapor removal from humid air and gases, Sep. Purif. Technol. 202 (2018) 345–356, https://doi.org/10.1016/J.SEPPUR.2018.03.005.
[46] M.A. Abdulhamid, G. Genduso, Y. Wang, X. Ma, I. Pinnau, Plasticization-Resistant carboxyl-functionalized 6FDA-polyimide of intrinsic microporosity (PIM-PI) for membrane-based gas separation, Ind. Eng. Chem. Res. 59 (2020) 5247–5256, https://doi.org/10.1021/ACS.IECR.9B04994.
[47] S.-H. Park, K.-J. Kim, W.-W. So, S.-J. Moon, S.-B. Lee, Gas separation properties of 6FDA-based polyimide membranes with a polar group, Macromol. Res. 11 (2003) 157–162.
[48] L. Wang, Y. Cao, M. Zhou, S.J. Zhou, Q. Yuan, Novel copolyimide membranes for gas separation, J. Membr. Sci. 305 (2007) 338–346, https://doi.org/10.1016/J.MEMSCI.2007.08.024.
[49] S.P. Liu, C.W. Liang, Preparation and mechanical properties of polypropylene/montmorillonite nanocomposites - after grafted with hard/soft grafting agent, Int. Commun. Heat Mass Tran. 38 (2011) 434–441, https://doi.org/10.1016/J.ICHEATMASSTRANSFER.2010.12.030.
[50] T.-H. Bae, J. Suk Lee, W. Qiu, W.J. Koros, C.W. Jones, S. Nair, T. Bae, J.S. Lee, W. Qiu, W.J. Koros, C.W. Jones, S. Nair, A high-performance gas-separation membrane containing submicrometer-sized metal–organic framework crystals, Angew. Chem. Int. Ed. 49 (2010) 9863–9866, https://doi.org/10.1002/ANIE.201006141.

[51] F. Cacho-Bailo, G. Caro, M. Etxeberría-Benavides, O. Karvan, C. Téllez, J. Coronas, MOF–polymer enhanced compatibility: post-annealed zeolite imidazolate framework membranes inside polyimide hollow fibers, RSC Adv. 6 (2016) 5881–5889, https://doi.org/10.1039/C5RA26076K.
[52] J.E. Bachman, J.R. Long, Plasticization-resistant Ni2(dobdc)/polyimide composite membranes for the removal of CO2 from natural gas, Energy Environ. Sci. 9 (2016) 2031–2036, https://doi.org/10.1039/C6EE00865H.
[53] K. Tanaka, M. Okano, H. Toshino, H. Kita, K. I.Okamoto, Effect of methyl substituents on permeability and permselectivity of gases in polyimides prepared from methyl-substituted phenylenediamines, J. Polym. Sci. B Polym. Phys. 30 (1992) 907–914, https://doi.org/10.1002/POLB.1992.090300813.
[54] B. Zornoza, C. Téllez, J. Coronas, O. Esekhile, W.J. Koros, Mixed matrix membranes based on 6FDA polyimide with silica and zeolite microsphere dispersed phases, AIChE J. 61 (2015) 4481–4490, https://doi.org/10.1002/AIC.15011.
[55] J.H. Kim, W.J. Koros, D.R. Paul, Effects of CO2 exposure and physical aging on the gas permeability of thin 6FDA-based polyimide membranes: Part 1. Without crosslinking, J. Membr. Sci. 282 (2006) 21–31, https://doi.org/10.1016/J.MEMSCI.2006.05.004.
[56] S. Asensio-Delgado, F. Pardo, G. Zarca, A. Urtiaga, Absorption separation of fluorinated refrigerant gases with ionic liquids: equilibrium, mass transport, and process design, Sep. Purif. Technol. 276 (2021) 119363, https://doi.org/10.1016/J.SEPPUR.2021.119363.
[57] K.S.W. Sing, D.H. Everett, R.A.W. Haul, L. Moscou, R.A. Pierotti, J. Rouquerol, T. Siemieniewska, Reporting physisorption data for gas/solid systems with special reference to the determination of surface area and porosity, Pure Appl. Chem. 57 (1985) 603–619, https://doi.org/10.1351/PAC198557040603.
[58] M. Thommes, K. Kaneko, A.V. Neimark, J.P. Olivier, F. Rodriguez-Reinoso, J. Rouquerol, K.S.W. Sing, Physisorption of gases, with special reference to the evaluation of surface area and pore size distribution (IUPAC Technical Report), Pure Appl. Chem. 87 (2015) 1051–1069, https://doi.org/10.1515/PAC-2014-1117.
[59] B. Abebe, H.C.A. Murthy, E. Amare, Summary on adsorption and photocatalysis for pollutant remediation: mini review, J. Encapsulation Adsorpt. Sci. 8 (2018) 225–255, https://doi.org/10.4236/jeas.2018.84012.
[60] M.M. Khan, K. Halder, S. Shishatskiy, V. Filiz, Synthesis and crosslinking of polyether-based main chain benzoxazine polymers and their gas separation performance, Polymers 10 (2018) 221, https://doi.org/10.3390/POLYM10020221. , Page 221 10 (2018).
[61] E.A. Guggenheim, Application of Statistical Mechanics, Clarendon Press, Oxford, 1966.
[62] M. Lanč, K. Pilnáček, C.R. Mason, P.M. Budd, Y. Rogan, R. Malpass-Evans, M. Carta, B.C. Gándara, N.B. McKeown, J.C. Jansen, O. Vopička, K. Friess, Gas sorption in polymers of intrinsic microporosity: the difference between solubility coefficients determined via time-lag and direct sorption experiments, J. Membr. Sci. (2019) 570–571, https://doi.org/10.1016/J.MEMSCI.2018.10.048, 522–536.
[63] O. Vopička, K. Friess, Analysis of gas sorption in glassy polymers with the GAB model: an alternative to the dual mode sorption model, J. Polym. Sci. B Polym. Phys. 52 (2014) 1490–1495, https://doi.org/10.1002/POLB.23588.
[64] O. Vopička, M. Lanč, K. Friess, Phenomenology of vapour sorption in polymers of intrinsic microporosity PIM-1 and PIM-EA-TB: envelopment of sorption isotherms, Curr Opin Chem Eng 35 (2022) 100786, https://doi.org/10.1016/J.COCHE.2021.100786.
[65] A. Tariq, N.M. Ahmad, M.A. Abbas, M.F. Shakir, Z. Khaliq, S. Rafiq, Z. Ali, A. Elaissari, Reactive extrusion of maleic-anhydride-grafted polypropylene by torque rheometer and its application as compatibilizer, Polymers 13 (2021) 1–17, https://doi.org/10.3390/POLYM13040495.
[66] P. Amirabedi, A. Akbari, R. Yegani, Fabrication of hydrophobic PP/CH3SiO2 composite hollow fiber membrane for membrane contactor application, Sep. Purif. Technol. 228 (2019), https://doi.org/10.1016/J.SEPPUR.2019.115689.
[67] B. Haider, M.R. Dilshad, M. Atiq Ur Rehman, J. Vargas Schmitz, M. Kaspereit, Highly permeable novel PDMS coated asymmetric polyethersulfone membranes loaded with SAPO-34 zeolite for carbon dioxide separation, Sep. Purif. Technol. 248 (2020) 116899, https://doi.org/10.1016/J.SEPPUR.2020.116899.
[68] M. Rezakazemi, A. Vatani, T. Mohammadi, Synergistic interactions between POSS and fumed silica and their effect on the properties of crosslinked PDMS nanocomposite membranes, RSC Adv. 5 (2015) 82460–82470, https://doi.org/10.1039/C5RA13609A.
[69] X.H. Do, Q.T. Nguyen, S. Kim, A.S. Lee, K.Y. Baek, Effect of thermal processing on brominated 6FDA-DAM for effective propylene/propane separation, Sep. Purif. Technol. 262 (2021) 118331, https://doi.org/10.1016/J.SEPPUR.2021.118331.
[70] M. Safak Boroglu, A.B. Yumru, Gas separation performance of 6FDA-DAM-ZIF-11 mixed-matrix membranes for H2/CH4 and CO2/CH4 separation, Sep. Purif. Technol. 173 (2017) 269–279, https://doi.org/10.1016/J.SEPPUR.2016.09.037.
[71] E.S. Sanders, Penetrant-induced plasticization and gas permeation in glassy polymers, J. Membr. Sci. 37 (1988) 63–80, https://doi.org/10.1016/S0376-7388(00)85069-3.
[72] S. Velioğlu, M.G. Ahunbay, S.B. Tantekin-Ersolmaz, Investigation of CO2-induced plasticization in fluorinated polyimide membranes via molecular simulation, J. Membr. Sci. 417 (418) (2012) 217–227, https://doi.org/10.1016/J.MEMSCI.2012.06.043.
[73] G. Liu, Y. Labreche, N. Li, Y. Liu, C. Zhang, S.J. Miller, V.P. Babu, N. Bhuwania, W. J. Koros, Simultaneously tuning dense skin and porous substrate of asymmetric hollow fiber membranes for efficient purification of aggressive natural gas, AIChE J. 65 (2019) 1269–1280, https://doi.org/10.1002/AIC.16520.